J Sol-Gel Sci Technol (2012) 61:355–361
DOI 10.1007/s10971-011-2634-1

ORIGINAL PAPER

Nano-sized blue spectral shift in sol–gel derived mesoporous titania films

P. Karasiński · E. Gondek · S. Drewniak · I. V. Kityk

Received: 23 April 2011 / Accepted: 21 November 2011 / Published online: 6 December 2011

Abstract Following the spectral energy shift of the energy gap (blue shift) of the TiO_2 sol–gel derived films we have evaluated diameters of the nanocrystallites. The TiO_2 films were deposited by dip-coating technique. Two types of mesoporous films were studied: films with porosity ~16% and refractive index (2.15 at wavelength 633 nm) and films with porosity ~46% and refractive index (1.61 at wavelength 633 nm). High porosity and consequently low refractive index was achieved by adding the non-ionic surfactant Triton X-100 to the starting solution as template. The principal goal of the work is to establish the influence of the Triton X-100 on the morphology as well as to establish a possible correlation between the morphology and optical features of the titania films. The surface morphology was explored using AFM method. And the energy gap was determined from the transmission spectra. Analysis of the blue energy spectral shift is performed following the excitonic model.

Keywords Sol–gel · Titanium dioxide · Nano confined effects · Anatase · Band energy gap

P. Karasiński · S. Drewniak
Department of Optoelectronics, Silesian University of Technology, ul. Krzywoustego 2, 44-100 Gliwice, Poland

E. Gondek (✉)
Institute of Physics, Technical University of Krakow, ul. Podchorążych 1, 30-084 Krakow, Poland
e-mail: gondek69@gmail.com

I. V. Kityk
Electrical Engineering Department, Czestochowa University Technology, Armii Krajowej 17, Czestochowa, Poland

1 Introduction

Titanium dioxide TiO_2 is a promising optoelectronic wide energy band gap semiconductor oxide film. It is of interest for use as gas sensor [1, 2], photoinduced optical operated materials [3], solar cell [4–6], photocatalyst [7–9], self-cleaning glasses [10], electrochromic films [11], antireflection coatings [12] and transparent conductors [13]. Titanium dioxide is also a principal component used in planar waveguide technology [14, 15]. Several synthesis methods concerning titanium dioxide thin films are described in the literature, such as *e*-beam evaporation [2], magnetron sputtering [7, 16], ultrasonic spray pyrolysis [17], chemical vapor deposition [18, 19], metal organic chemical vapor deposition [13], pulsed laser deposition [20], and sol–gel method [1, 5, 6, 9–13]. The sol–gel method has advantages, due to low temperature processing, easy coating of large area, and being suitable for preparation of porous films and homogeneous multicomponent oxide films. The most important advantage of sol–gel over conventional coating methods is the ability to tailor the microstructure of deposited films [21], so using the sol–gel method one can produce titania films with desirable structure. Contrary to the other, the sol–gel method is very efficient and does not require an expensive technological equipment.

In this study, the surface morphology and optical properties near the band energy gap edge for sol–gel derived TiO_2 films deposited on soda-lime glass substrates were studied. The films were prepared by the dip coating method. Two types of the films were studied: compact films with refractive index of ~2.15 and mesoporous films with refractive index of ~1.61 (at wavelength 633 nm). High porosity and consequently low refractive index was achieved by adding of the non-ionic surfactant Triton

X-100 to the initial solution as template. The principal goal of the work is to establish the influence of the Triton X-100 on the morphology as well as to study a possible correlation between the morphology and optical features of the titania films.

2 Experimental procedures

2.1 Films fabrication

The principal processes of sol–gel technology are described in detail by Brinker and Scherer [21]. The major problems in texturing titania is the high reactivity of Ti alkoxide precursors towards to rapid hydrolysis and condensation reactions. Rapid condensation processes lead to the formation of oxo-oligomers, clusters or small polymers prior to the formation of the textured template. However, the control of hydrolysis and condensation, through the addition of condensation inhibitors such as chelating agents or mineral acids, can overcome the problem [21–23]. As a consequence in the presented here research, the titania films were fabricated using the tetraethoxyorthotitanate $Ti(OEt)_4$ (TET) as a precursor for titania, water H_2O, ethyl alcohol C_2H_5OH (EtOH) as homogenizing agent and hydrochloric acid HCl as a condensation inhibitor. Two types of gel were synthesized, which were used for synthesis of the TiO_2 films possessing different porosity and refractive indices.

The first sol, which will be indicated as sol-A, was prepared with the following molar ratios of the components: TET:EtOH:H_2O:HCl = 1:15:2.8:0.7. The second one, which will be indicated as sol-B, has been prepared similarly to the sol-A. To the sol-B it was additionally added acetylaceton (Acac) as a chelate and non-ionic surfactant Triton X-100 as a template. Tetraethoxytitanate was mixed with acetylaceton in the molar ratio TET:Acac = 1:1. A non-ionic surfactant Triton X-100 was added in the volume ratio TET:Triton X-100 = 1:0.5. to the starting solutions. After mixing of the components, the sols formation was performed during 3 h in a sealed glass crucible at temperature about 50 °C, using ultrasonic mixing. Ultra clean soda-lime glass substrates (microscope slides, Menzel-Glaser), was cleaned by a method described in the Ref. 15. The films were deposited on the cleaned substrates by dip coating method. The such prepared film were annealed at temperature of 500 °C during 1 h. For the substrate withdrawal speed from the sol-A of 1.7 ÷ 3.0 cm/min we have obtained films with thickness varying within 71–89 nm. For sol-B and the same withdrawal speed we have synthesized films with thickness varying within 113–130 nm. Sol-B containing Triton X-100 had higher viscosity with respect to sol-A. As a consequence, the thickness of the film fabricated from sol B is higher than those one fabricated from sol A at the same withdrawal rate of substrate.

At the beginning precursor was solvated in water-less ethanol and afterwards HCl acid was added successively. The chemical reactions in the $Ti(OR)_4$/EtOH/H_2O/HCl were studied in details by Soler-Illia and co-workers [22–24]. Upon dissolution, $Ti(OR)_4$ precursors undergo fast exchange reactions with EtOH and HCl molecules, leading to formation of $Ti(OR)_{n-x}(OEt)_x$, $TiCl_{n-x}(OEt)_x$ nanoclusters, or a mixture of both. Subsequently, polycondensation reactions between metal alkoxides can occur, yielding metal-oxo condensates with general formula $Ti(OR)_x(OH)_yO_{2-(x+y)/2}$ or $TiCl_x(OH)_yO_{2-(x+y)/2}$. Typically, $x \approx 0.3-0.7$ and $y \approx 0-0.2$; while the value of y increases with the water content, x decreases [22–24].

The role of Triton X-100 as a surfactant has been described by Avnir and co-workers in Ref. [25]. Dag and co-workers have fabricated mesoporous TiO_2 using $Ti(OEt)_4$ as precursor and non-ionic surfactant $CH_3(CH_2)_n(OCH_2CH_2)_mOH$ [26], which is similar to Triton X-100. Their studies have shown that appeared nanoclusteres during process of controlled $Ti(OEt)_4$ effectively interact with surfactant $CH_3(CH_2)_n(OCH_2CH_2)_mOH$ which favors formation of nanoclaster/non-ionic surfactant "titanotropic" mesophase that undergoes hydrolytic polycondensation to give mesostructured titania with a wormhole structure, an amorphous titania framework, and uniform pore size distribution. The surfactant pre-organizes the clusters, which are attached to its head group [26]. We assume that for the case of use the Triton X-100 the similar reaction should be observed.

2.2 Sample characterization

The such prepared surface of the TiO_2 films have been monitored by atomic force microscope (AFM), using Ntegra Prima (NT-MDT), monochromatic ellipsometer Sentech SE400 (Sentech, model 2003, Germany). Additionally spectrophotometer UV–VIS HR4000CG (OceanOptics) with spectral resolution 0.75 nm within 200–1,100 nm spectral wavelength range was used. The AFM experiments for TiO_2 thin films were performed using semi-contact mode AFM. In AFM measurements the HA_NC (NT-MDT) silicon cantilever with nominal curvature radius of a tip equal to 10 nm and resonance frequency of 250 kHz was used. The AFM image analysis was carried out using commercial NOVA 1.0.26.1644 (NT-MTD) software procedures to evaluate Root-Mean-Square (RMS) surface roughness. The ellipsometric measurements were done for wavelength of He–Ne cw laser $\lambda = 633$ nm and spectroscopic measurements were carried out in the spectra range within 200–1,100 nm.

3 Results and discussion

3.1 Surface morphology

Figure 1 shows typical semi-contact AFM images of surface of the studied titania film fabricated from sol-A. Such titania films exhibit typical grain-type surface morphology. Following the Fig. 1a one can see clear aggregates possessing diameters equal of about 240 nm. More detailed analysis is presented in the Figs. 1b and 2a, which clarify that such aggregates are built from the less grains. The root mean square surface roughness is 0.88 nm over a 0.5×0.5 μm^2 area. Figure 2b shows a line profile taken along the surface presented in Fig. 2a. It is the same surface as presented in Fig. 1. The maximum grain height is equal to about 7 nm, while the maximum grain width for this film is equal to about 35 nm.

Figure 3 shows typical semi-contact AFM images of surface for the titania film fabricated from sol B. It is clear seen that in this case the surface of the film is more rough with respect to the film originated from gel A (Fig. 1). It is visible, that the film has a grain structure. The root mean square surface roughness is 2.70 nm over a 0.5×0.5 μm^2 area.

Figure 4b shows a line profile taken along the surface presented in Fig. 4a. It is the same surface as presented in Fig. 3. The maximum grain height is estimated to be about 12 nm, while the maximum grain width for this film is equal to about 38 nm. One can clearly see that for the two types of layers the grain diameters are comparable, however the maximal heights of the grains for the film produced from sol-B are substantially higher with respect to those obtained from sol-A.

The presented here results concerning the AFM demonstrate substantial influence of non-ionic surfactant Triton X-100 on the morphology if the such synthesized films. In the layers formed in sol B containing surfactant the grains do not form the aggregates, on the contrary to the layer formed from sol A (see Fig. 1). The surfactant decreases the capillary stresses and avoids a destroying of the layered structure during drying process [25]. As a consequence the layer structure is more modified and its surface is more rough. For both types of the layers the maximal grain sizes are comparable, however, the maximal heights of grains are substantially different. The lower maximal values of grain heights (about 7 nm) for the layers formed from sol A without surfactant are caused by effect of collapse of structure for the layers formed from A during the drying and annealing processes.

3.2 Optical features

Refractive index of films fabricated from sol-A was equal to about 2.15 (at wavelength 632.8 nm) and ones fabricated

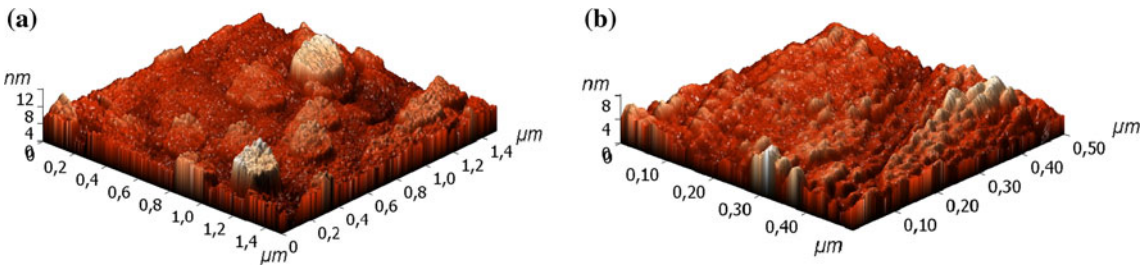

Fig. 1 AFM topographical images (at different magnification) of TiO_2 thin film deposited on soda-lime glass substrates obtained by sol–gel dip coating process: **a** the scale correspond to 1.5×1.5 μm^2, **b** the scale correspond to 0.5×0.5 μm^2

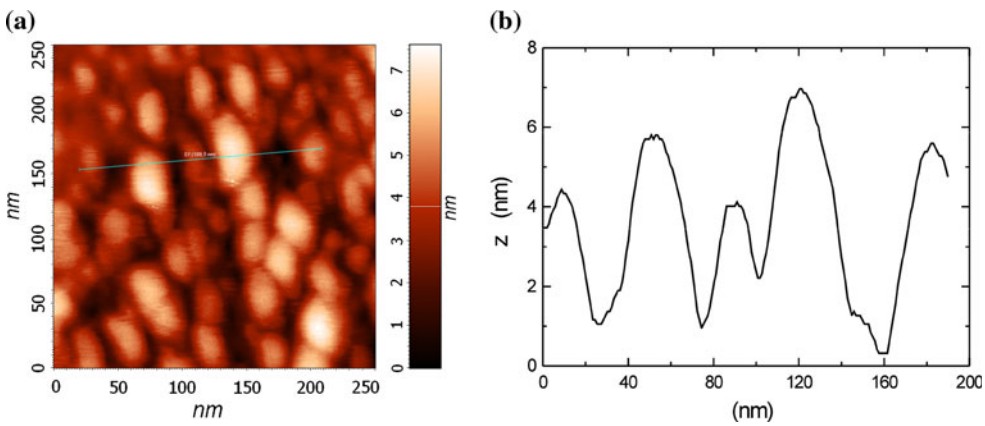

Fig. 2 Typical AFM topographical image of TiO_2 thin films (**a**) and corresponding surface profile (**b**)

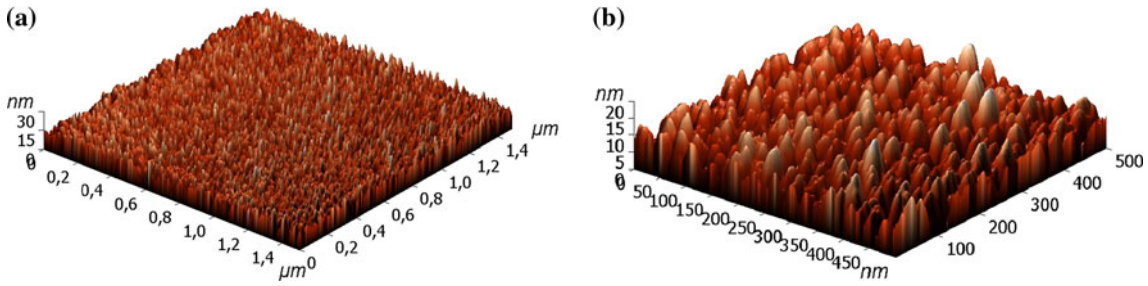

Fig. 3 AFM topographical image (at different magnification) of TiO_2 thin films deposited on soda-lime glass substrates by sol–gel dip coating process. **a** the scale correspond to 1.5 × 1.5 μm^2, **b** the scale correspond to 0.5 × 0.5 μm^2

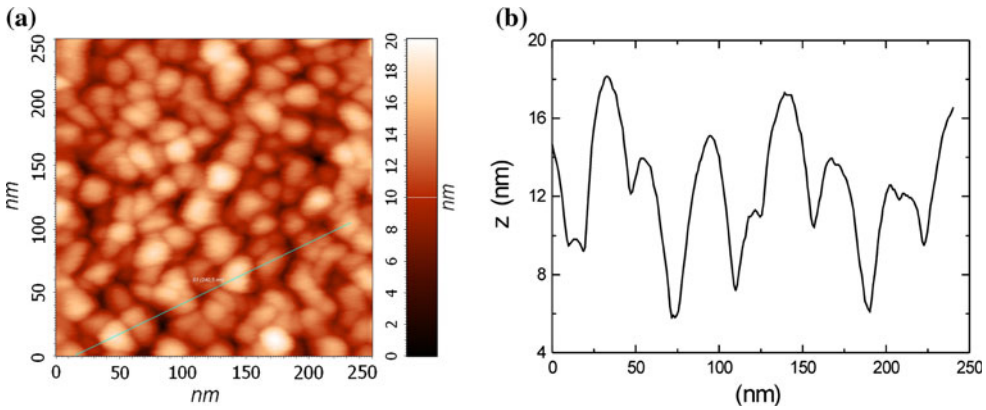

Fig. 4 AFM topographical image of TiO_2 thin films (**a**) and surface profile (**b**)

from sol-B was equal about 1.61 (at wavelength 632.8 nm). Using the measured values n of the refractive index of the fabricated titania films, their volume percentage porosity P was determined. For this purpose, the Lorentz-Lorenz equation was applied:

$$\frac{n^2-1}{n^2+2}=\left(1-\frac{P}{100\%}\right)\frac{n_d^2-1}{n_d^2+2} \quad (1)$$

where n_d is the refractive index of anatase $\approx$ 2.52 (at wavelength 632.8 nm). So one can assume that in the presented here layers, which are annealed at temperature 500 °C there is present only anatase [3]. Rutyl appears in the layers of TiO_2which are thermoannelaed at temperatures higher 600 °C [17, 27, 28]. Assuming that the pores of these layers are filled up solely with air, their porosity calculated on the basis of (1) is $P_A \approx 16\%$ for films fabricated from sol-A and $P_B \approx 46\%$ for films fabricated from sol-B. Using the simplified effective medium approximation (EMA) $n = n_{air}P + n_d(1 - P)$ with $n_{air} = 1$ the porosity are equal to $P_A = 24\%$ and $P_A = 60\%$, respectively. So the determined porosity is dependent on the used model of EMA. The difference between porosities obtained from various EMA models can be significant and increase as the index of refraction of the continuous phase material increases [29]. The review of EMA models is presented in Ref. [30].

Figure 5 shows the transmittance spectra of titania films fabricated from the sol-A. Every spectral curve clearly shows the occurred interference patterns. It can be observed that with the increase of the thickness d of the titania film, its refractive index n is increasing because increased coating rates (increased film thickness) results in particle ordering [21].

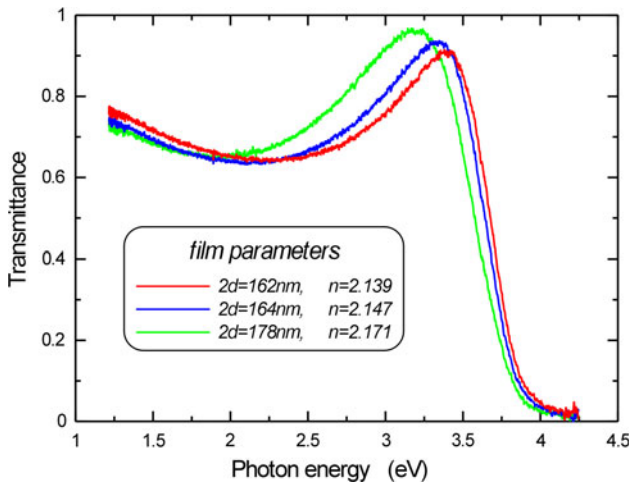

Fig. 5 Transmittance spectra of compact titania films

In order to determine the optical band energy gap of the TiO_2 films the absorption coefficient α of the film was evaluated from the transmittance T of the film and its thickness d:

$$\alpha = -\frac{1}{d}\ln(T) \tag{2}$$

The transmittance was experimentally evaluated from the UV–Vis spectra. If to assume parabolic energy distribution of density of states for valance and conducting band, the E_g of the titania films was determined by analysing the relationship between absorption coefficient α and photon energy hv using Tauc equation [31]:

$$\alpha(hv) = \frac{C\left(hv - E_g\right)^{a/2}}{hv} \tag{3}$$

where E_g is a bend gap of the material, C is a constant, and $a = 1$ for direct transition between the edges of valence and the conduction bend and $a = 4$ for indirect transition. The energy gaps value are determined by extrapolation of the linear part of the plots of the absorption coefficient $(\alpha hv)^{2/a}$ versus photon energy hv.

The Fig. 6 presents the dependence of the $(\alpha hv)^2$ versus photon energy. One can see that the TiO_2 possess the direct energy gap ($a = 1$). Because the dip coating method gives a possibility to obtain the films from two sides of the substrate the energy gap was determined from summary film thickness $2d = 162$ nm and the energy gap was equal to $E_g = 3.749$ eV. In turn for the films with total $2d = 178$ nm the energy gap was equal to $E_g = 3.720$ eV. So one can clearly see that with the decreasing of film thickness occurs energy gap is increasing. It is a consequence of the varying materials structure with the varying thickness. The thicker sol layers are dried more quickly, so the TiO_2 particle after crystallization may form higher nanocrystallites, with the lower energy gaps E_g. The evaporation of the solvents from the layer favours the changes of their features, which may cause a restraining of nanocrystallite growth.

The transmittance spectra of the mesoporous films TiO_2, formed by gel B are presented in the Fig. 7. For this case thicknesses of the layers are substantially higher with respect to the synthesized from sol A (Fig. 5). However, the maximums and minimums of the interference are weakly visible. It is a consequence of light depolarization in the studied materials. In Ref [32]. it was shown that the porous layers demonstrate strong depolarized features. It can be observed that with the increase of the thickness d of the porous titania film, its refractive index n is decreasing. Such dependence are typical for a polymeric sol, where the polymers are weakly charged and the condensation rate is high [21].

Figure 8 presents the spectral dependences of the normalized absorption coefficient. It is a principal difference because there occurs the indirect inter-band transition ($a = 4$) edge $E_g = 3.40$ eV.

For the two studied types of films the energy gaps are higher with respect to the energy gap of the bulk anatase specimens $E_{bulk} = 3.20$ eV. This is a consequences of quantum size effects [33–37]. It is crucial that following the values of spectral shift (blue energy shift) of the energy gap one can evaluate the diameters of the crystallites.

For parabolic energy band near the band-gap, the average value of the crystallite diameter $2R$ may be estimated from the formula [34–36, 40]:

$$\Delta E = \frac{\pi^2\hbar^2}{2R^2}\left[\frac{1}{m_e} + \frac{1}{m_h}\right] - 1.786\frac{e^2}{4\pi\varepsilon\varepsilon_0 R} - 0.248E^*_{Ry} \tag{4}$$

where $\hbar = 1.0545 \times 10^{-34}$Js is the reduced Planck's constant, m_e is the effective mass of the electron, m_h is the effective mass of the hole, ε_0 is the permittivity of free space, ε is the dielectric constant of anatase TiO_2, $E^*_{Ry} = e^4/\left(2\varepsilon^2\hbar^2\left(m_e^{-1} + m_h^{-1}\right)\right)$ is the effective Rydberg energy. ΔE is a blue shift of the band-gap energy results of two

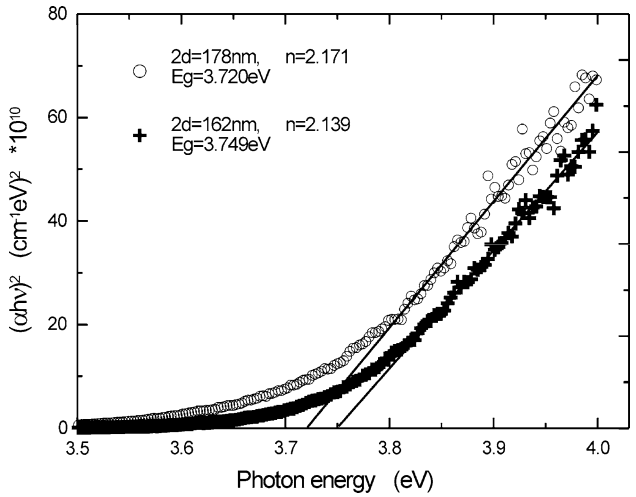

Fig. 6 Dependence of absorption coefficient $(\alpha hv)^2$ vs. photon energy

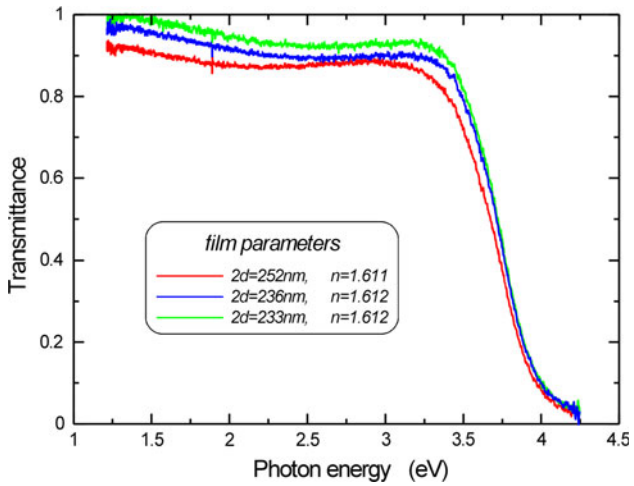

Fig. 7 Transmittance spectra of mesoporous titania films

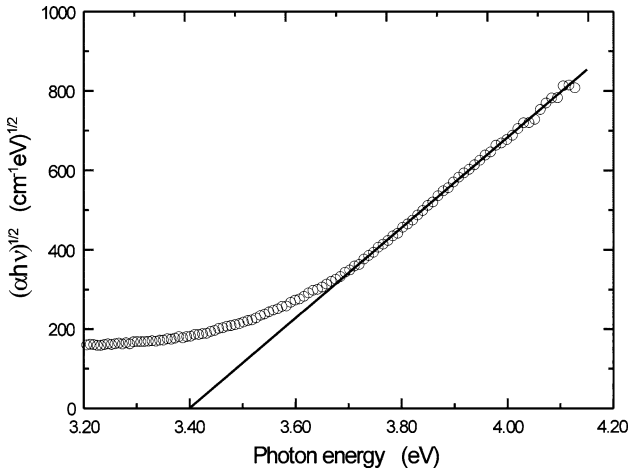

Fig. 8 Absorption coefficient $(\alpha h\nu)^{1/2}$ vs. photon energy

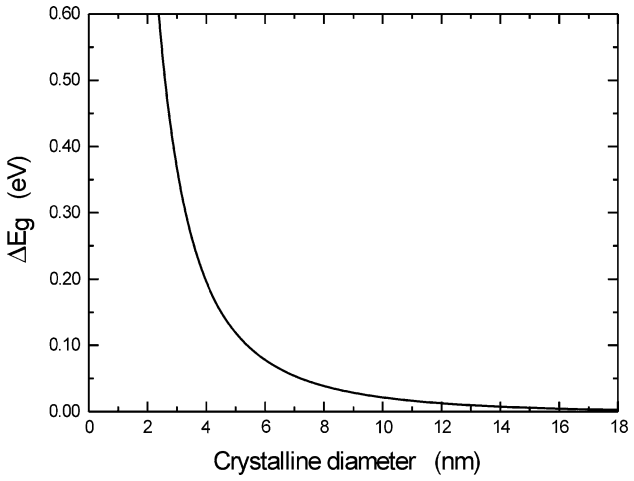

Fig. 9 Energy band gap shift vs. crystalline diameter $2R$

competing mechanisms: a widening due to the Burstein-Moss effect, and a narrowing due electron–electron and electron–ion scattering [38, 41].

Figure 9 shows calculated dependence blue shift band gap energy on the crystalline size ($2R$) calculated on the base Eq. 4. In the calculations we have been taken into account the parameters as follow; effective masses of the electron $m_e = m_0 = 9.11 \times 10^{-31}$ kg and the hole $m_h = 0.65\ m_0$ [39], dielectric constant of anatase $\varepsilon = 31$.

For the titania films fabricated from sol-A the blue energy shift is in the range 0.52–0.55 eV, but for the titania films fabricated from sol-B the blue energy shift is about 0.2 eV. Following the dependences presented in the Fig. 9 we have determined diameters of the anatase nanocrystallites, which were equal to $2R \approx 2.5$ nm for the layers produced from sol A and $2R \approx 4$ nm for the layers synthesized fir sol-B. As a consequence the grains presented in the figures (Sect. 3.1) have the polycrystalline structure. So one can see that presence of Triton X-100 leads not only to higher roughness of the synthesized layers, however, also to higher diameters of anatase nanocrystallites.

The effective Bohr radius of the exciton calculated from the formula [36, 37]:

$$a_B = \frac{\hbar\varepsilon\varepsilon_0}{e^2}\left[\frac{1}{m_e} + \frac{1}{m_h}\right] \tag{5}$$

is $a_B = 0.823$ nm.

From these equation one can see that the exciton radius is less from the estimated radiuses R of nanocrystallites for the studied samples.

4 Conclusion

We have established the influence of the Triton X-100 on the morphology as well as on optical features of the titania films. The blue spectral shift of energy gap was determined for two types of TiO_2 films fabricated using sol–gel technology. The synthesized layers possessed the layers with refractive indices $\sim$2.15 i $\sim$1.61, respectively. The low refractive indices are caused by high porosity of the layers, which is achieved due to adding of surfactant Tryton X-100. We have established a crucial influence of the microstructure and morphology of the layers on the value of energy gap. The micro porous layers possessing the refractive indices 2.15 possesses the direct energy gap, which depending on the film thickness is varied within $E_g \approx 3.72 \div 3.75$ eV. The mesoporous films with refractive index 1.61 possess the indirect energy gap equal to $E_g \approx 3.40$ eV. So following the degree of porosity one can control their energy gap. The principal fact consists in an evaluation of the nano-grain sizes. Following the determined blue energy shift we have evaluated diameters of the anatase nanocrystallites, which for the mesoporous layers are equal to $\sim$4 nm, and for the low porous layers are equal to $\sim$2.5 nm. The presence of Triton X-100 causes higher roughness and higher nanocrystallite sizes.

References

1. Shimizu Y, Hyodo T, Egashira M (2004) Mesoporous semiconducting oxides for gas sensor application. J Eur Ceram Soc 24:1389–1398
2. Aroutiounian V, Arakelyan V, Galstyan V, Martirosyan K, Soukiassian P (2009) Hydrogen sensor made of porous silicon and covered by TiO_{2-x} or ZnO <Al> thin film. IEEE Sens J 9:9–12

3. Djaoued Y, Ozga K, Wojciechowski A, Reshak AH, Robichaud J, Kityk IV (2010) Photoinduced effect in TiO_2 nanocrystaline films with different morphology. J Alloys Compd 508:599–605
4. Hitosugi T, Yamada N, Nakao S, Hirose Y, Hasegawa T (2010) Properties of TiO_2-based transparent conducting oxides. Phys Status Solidi A 207:1529–1537
5. Chen D, Huang F, Cheng Y-B, Caruso RA (2009) Mesoporous anatase TiO_2 beads with high surface areas and controllable pore sizes: a superior candidate for high-performance dye-sensitized solar cells. Adv Mater 21:2206–2210
6. Ngamsinlapasathian S, Pavasupree S, Suzuki Y, Yoshikawa S (2006) Dye-sensitized solar cell made of mesoporous titania by surfactant-assisted templating metod. Sol Energy Mater Sol Cells 90:3187–3192
7. Miao L, Tanemura S, Kondo Y, Iwata M, Toh S, Kaneko K (2004) Microstructure and bactericidal ability of photocatalitic TiO_2 thin films prepared by rf helicon magnetron sputtering. Appl Surf Sci 238:125–131
8. Shibata H, Ohshika S, Ogura T, Watanabe S, Nishio K, Sakai H, Abe M, Hashimoto K, Matsumoto M (2011) Preparation and photocatalytic activity under visible light irradiation of mesostructured titania particles modified with phthalocyanine in the pores. J Photochem Photobiol A Chem 217:136–140
9. Liu W, Zou B, Zhao J, Cui H (2010) Optimizing sol-gel infiltration for the fabrication of high-quality titania inverse opal and its photocatalytic activity. Thin Solid Films 518:4923–4927
10. Mellott NP, Durucan C, Pantano CG, Guglielmi M (2006) Commercial and laboratory prepared titanium dioxide thin films for self-cleaning glasses: photocatalytic performance and chemical durability. Thin Solid Films 502:112–120
11. Dinh NN, Th N, Oanh T, Long PD, Bernard MC, Hugot-Le Goff A (2003) Electrochromic properties of TiO_2 anatase thin films prepared by a dipping sol–gel method. Thin Solid Films 423: 70–76
12. Jin P, Miao L, Tanemura S, Xu G, Tazawa M, Yoshimura K (2003) Formation and characterization of TiO_2 thin films with application to a multifunctional heat mirror. Appl Surf Sci 212–213:775–781
13. Chen D, Xu G, Miao L, Chen L, Nakao S, Jin P (2010) W-doped anatase TiO_2 transparent conductive oxide films: theory and experiment. J Appl Phys 107:063707
14. Karasiński P (2011) Embossable grating couplers for planar evanescent wave sensors. Opto-Electron Rev 19:13–24
15. Karasiński P, Tyszkiewicz C, Rogoziński R, Jaglarz J, Mazur J (2011) Optical rib waveguides based on sol-gel derived silica-titania films. Thin Solid Films 519:5544–5551
16. Ranade AN, Fulton C, Seebergh JE, Nichols M, Remillard J, Graham M, Chung Yip-Wah (2010) Synthesis, structure, and optical properties of Au–TiO2 composite thin films. Thin Solid Films 519:1490–1494
17. Nakaruk A, Ragazzon D, Sorrell CC (2010) Anatase-rutile transformation through high-temperature annealing of titania films produced by ultrasonic spray pyrolysis. Thin Solid Films 518:3735–3742
18. Zhang WZ, Zhang T, Yin W, Cao GY (2007) Relationship between photocatalytic activity and structure of TiO_2 thin film. Chin J Chem Phys 20:95–98
19. Babelon P, Dequiedt AS, Mostéfa-Sba H, Bourgeois S, Sibillot P, Sacilotti M (1998) SEM and XPS studies of titanium dioxide thin films grown by MOCVD. Thin Solid Films 322:63–67
20. Tao RH, Wu JM, Xue HX, Dong WW, Deng ZH, Fang XD (2010) Pulsed laser deposition of titania on rutile nanorod arrays. Thin Solid Films 518:4191–4196
21. Brinker CJ, Scherer GW (1990) Sol-gel science: the physics and chemistry of sol-gel processing. Academic Press, San Diego, CA
22. Soler-Illia GJ de AA, Scolan E, Louis A, Albouy PA, Sanchez C (2001) Design of meso-structured titanium oxo based hybrid organic-inorganic networks. New J Chem 25: 156–165
23. Soler-Illia GJ de AA, Sanchez C (2000) Interactions between poly(ethylene oxid)-based surfactants and transition metal alkoxides: their role in the templated construction of mesostructured hybrid organic-inorganic composites. New J Chem 24:493–499
24. Soler-Illia GJ de AA, Louis A, Sanchez C (2002) Synthesis and characterization of mesostructured titania-based materials through evaporation-induced self-assembly. Chem Mater 14: 750–759
25. Avnir D, Kaufman VR, Reisfeld R (1985) Organic fluorescent dyes trapped in silica and silica-titania thin films by the sol-gel method. Photophysical, film and cage properties. J Non-Cryst Solids 74:395–406
26. Dag Ö, Soten I, Çelik Ö, Polarz S, Coombs N, Ozin GA (2003) Solventless acid-free synthesis of mesostructured titania: nanovessels for metal complexes and metal nanoclusters. Adv Funct Mater 13:30–36
27. Nakaruk A, Lin CY, Perera DS, Sorrell CC (2010) Effect of annealing temperature on titania thin films prepared by spin coating. J Sol-Gel Sci Technol 55:328–334
28. Kim DJ, Hahn SH, Oh SH, Kim EJ (2002) Influence of calcination temperature on structural and optical properties of TiO_2 thin films prepared by sol–gel dip coating. Mater Lett 57:355–360
29. Braun MM, Pilon L (2006) Effective optical properties of non-absorbing nanoporous thin films. Thin Solid Films 496:505–514
30. Hutchinson NJ, Coquil T, Richman EK, Tolbert SH, Pilon L (2010) Reflectance of surfactant-templeted mesoporous silica thin films: Simulations versus experiments. Thin Solid Films 518: 2134–2140
31. Tauc J (1974) Amorphous and semiconductors. Plenum, London
32. Karsińskai P, Jaglarz J, Reben M, Skoczek E, Mazur J (2011) Porous silica xerogel films as antireflective coatings: fabrication and characterization. Opt Mater 33:1989–1994
33. Brus LE (1983) A simple model for the ionization potential, electron affinity, and aqueous redox potentials of small semiconductor crystallites. J Chem Phys 79:5566–5571
34. Bruc L (1986) Zero-Dimensional "Excitons" in semiconductor clusters. IEEE J Quantum Electron 22:1909–1914
35. Brus LE (1984) Electron-electron and electron-hole interactions in small semiconductor crystallites: the size dependence of the lowest excited electronic state. J Chem Phys 80:4403–4409
36. Kayanuma Y (1988) Quantum-size effects of interacting of electrons and holes in semiconductor microcrystals with spherical shape. Phys Rev B 38:9797–9805
37. Wang Y, Herron N (1991) Nanometer-sized semiconductor clusters: materials syntesis, quantum size effects, and photo physical properties. J Phys Chem 95:525–532
38. Hamberg I, Granqvist CG (1986) Evaporated Sn-doped In_2O_3 films: basic optical properties and applications to energy-efficient windows. J Appl Phys 60:R123–R159
39. Lee S, Cho IS, Noh JH, Hong KS, Han GS, Jung HS, Jeong S, Lee C, Shin H (2010) Correlation of anatase particle size with photocatalytic properties. Phys Status Solidi A 207:2288–2291
40. Reddy KM, Monorama SV, Reddy AR (2002) Bandgap studies on anatase titanium dioxide nanoparticles. Mater Chem Phys 78:230–245
41. Kityk IV, Demianiuk M, Majchrowski A, Ebothe J, Siemion P (2004) IR-induced second-harmonic generation in PbSe microcrystallites. J Phys Condens Mater 16:3533–3544